1-1-2013

Evidence for Antarctic Ice Sheets During the Late Eocene

Brian Smith
University of South Carolina

Evidence for Antarctic Ice Sheets During the Late Eocene.

by

Brian William Smith

Bachelor of Science
University of South Carolina, 2013

Submitted in Partial Fulfillment of the Requirements

For the Degree of Master of Science in

Marine Science

College of Arts and Sciences

University of South Carolina

2013

Accepted by:

Howie Scher, Major Professor

Michael Bizimis, Reader

Dave Barbeau, Reader

Lacy Ford, Vice Provost and Dean of Graduate Studies

DEDICATION

To Mom, Dad, Kim, and Erin, thank you for the continuous support and love.

ACKNOWLEDGEMENTS

I would like to thank my advisor and committee members for their expertise, guidance, and patience.

ABSTRACT

Previous studies of sediment from southern Kerguelen Plateau have provided insight about Antarctica's climate activity during the Bartonian/Priabonian boundary (ca. 37 Ma). Detrital and fossil fish tooth neodymium (Nd) isotope records, along with foraminiferal $\delta^{18}O$ values, suggest a change in the source of terrigenous sediment coincident with global cooling and/or ice sheet growth on Antarctica. My thesis work has corroborated the initial findings and has provided additional insight into the Antarctic weathering regime during this climate event. Nd and hafnium (Hf) isotope values of terrigenous sediment at ODP Site 748B (58°26.45'S, 78°58.89'E, 1290m) were cross-plotted along with the seawater and terrestrial array in Nd-Hf diagrams to constrain changes in the weathering style on Antarctica. The coupled Nd-Hf data suggests that the delivery of radiogenic isotope fingerprints to Kerguelen Plateau during the Bartonian/Priabonian boundary was a function of the style of weathering on Antarctica as well as modification of the terrigenous fraction during transport. An increased erosional flux of an older source is inferred from a decrease to more unradiogenic ε_{Nd} values 37 Ma. At the same time, there is a small shift in ε_{Hf}, to less radiogenic values, indicating a small change from chemical to mechanical style weathering. The findings support the conclusion that there was a change in

the Antarctic weathering flux, along with a change in weathering style approximately 37 Ma.

TABLE OF CONTENTS

DEDICATION iii

ACKNOWLEDGEMENTS iv

ABSTRACT v

LIST OF TABLES viii

LIST OF FIGURES ix

CHAPTER 1: INTRODUCTION 1

CHAPTER 2: METHODS AND MATERIALS 6

CHAPTER 3: RESULTS 8

CHAPTER 4: DISCUSSION 17

CHAPTER 5: CONCLUSION 21

REFERENCES 22

LIST OF TABLES

Table 3.1 Neodymium and Hafnium values from ODP Site 748B. 10

Table 3.2 Neodymium and Hafnium values from ODP Site 748B cont. 11

LIST OF FIGURES

Figure 3.1 Previous Bartonian/Priabonian Boundary isotope records. 12

Figure 3.2 Observed global Nd-Hf isotope systematics. 13

Figure 3.3 Sampling location on Kerguelen Plateau 14

Figure 3.4 Detrital ε_{Nd}, ε_{Hf}, and foraminifera $\delta^{18}O$ values 15

Figure 3.5 748B ε_{Nd} and ε_{Hf} values with seawater and terrestrial arrays 16

CHAPTER 1: INTRODUCTION

The earth's climate has undergone extreme changes over the past 65 million years. During the Eocene/Oligocene Transition 34 Mya, the earth cooled, and shifted from a "greenhouse earth" to an "icehouse earth" in a geologically short period of time. Ice sheet development during the Eocene Oligocene Transition (EOT) is supported by three types of proxies for global climate change; 1) a rapid deepening of the carbonate compensation depth (Lyle et al., 2005), 2) a eustatic sea level fall of 60 m, inferred from passive margin sequence stratigraphy (Miller et al., 2005), and 3) benthic foraminiferal $\delta^{18}O$ values increase, indicating cooling and ice sheet growth (Miller et al., 1987; Zachos et al., 2001; Coxall et al., 2005). Ice sheet development at the EOT was the culmination of a long term cooling trend, driven in large part by declining CO_2 levels (Pagani et al., 2005). It is thought that this large glaciation was preceded by smaller glacial events, but ice sheets during the late Eocene, and earlier, were likely too small to register in proxies for global climate change. This thesis will present evidence for enhanced weathering on Antarctica during the Bartonian/Priabonian boundary (37.2 Ma, within polarity chron C17n.1n) from a high latitude sediment core that can be linked to weathering/erosion by ice sheets during the "greenhouse" earth.

Preliminary data from southern Kerguelen Plateau (ODP Site 738, 62.7° S, 82.8° E, 2252 m; Figure 1) strongly indicates a change in Antarctic weathering

and or erosion at the Bartonian/Priabonian boundary (Scher et al., in prep). There is a benthic foraminiferal $\delta^{18}O$ shift of +0.4 ‰ indicating a cool event, and a minor decrease in bottom water ε_{Nd} values determined from fossil fish teeth (Munn, 2011), similar to what was observed during the EOT (Scher et al., 2011). The Nd isotopic composition (e.g., $^{143}Nd/^{144}Nd$, expressed as ε_{Nd} values, which are relative to the bulk earth) of terrigenous sediment (<63 μm fraction) is -12 before and after the event, but decreases to -15 during the cool event. The events observed on southern Kerguelen Plateau approximately 37 Ma provide evidence for a *ca.* 200 kyr glacial event on Antarctica (Scher et al., in prep).

In order to better constrain changes in Antarctic weathering during the Bartonian/Priabonian boundary, I produced coupled Nd-Hf isotope measurements from a sediment core on central Kerguelen Plateau (58°26.45'S, 78°58.89'E, 1290m). The results show a similar Nd isotope excursion to that observed on southern Kerguelen Plateau.

Furthermore, the coupled Nd-Hf results suggest differences in the style of weathering on Antarctica. Measurements of Nd-Hf have been used to define a seawater and terrestrial array in Nd-Hf diagrams (Figure 2). The terrestrial array consists of silicate rocks, oceanic rocks, sediments, and continental rocks; while ferromanganese crust/nodules and seawater define the seawater array (Albarede et al., 1998; Vervoort, 1999; van de Flierdt et al., 2007; Stichel et al., 2011). Van de Flierdt et al. (2007) showed that modern-day circum-Antarctic sediment plotted along the terrestrial array (Figure 2).

One explanation for the difference between the terrestrial and seawater arrays is the zircon effect. Zircons have low Lu/Hf values, which result in low 176/177 values (i.e., negative ε_{Hf} values). Zircons are also highly resistant to chemical weathering, and are generally retained on the continents during weathering and transport. Based on this paradigm, an increase in mechanical weathering by glacial grinding during the Eocene would mobilize zircon and its relatively less radiogenic ε_{Hf} values into the weathering flux ultimately to circum-Antarctic depocenters. Based on this interpretation of the seawater and terrestrial arrays we expect that terrigenous sediment will plot on the seawater array during times of low $\delta^{18}O$ (warmer, chemical weathering dominated), and on the terrestrial array during times of high $\delta^{18}O$ (cooler, relatively higher rates of mechanical weathering).

Two mineral reservoirs on Earth that contain hafnium are apatite and zircons. Apatite is more easily weathered mineral compared to zircon, and also has high $^{176}Lu/^{177}Hf$ ratios. Opposite of apatite, zircons have low $^{176}Lu/^{177}Hf$ ratios. This is because Hf atoms have a charge/radius profile that is readily interchanged with Zr in the zircon structure. Lu on the other hand, does not incorporate easily in zircon. This results in low $^{176}Lu/^{177}Hf$. Because of this, the in situ decay rate of Lu is negligible and results in low $^{176}Hf/^{177}Hf$. These attributes from zircon create the “zircon effect” (White et al., 1986). This effect explains the ε_{Hf} offset between the seawater and terrestrial array.

Zircons are minerals that are resistant to chemical weathering, and have recorded some of the earliest history of Earth. Zircons are particularly useful for

paleoceanography because they contain information on the Lu-Hf system. Unstable ^{176}Lu decays into ^{176}Hf and has a half-life of 35 billion years (Kinny, 2003). Having such a long half-life, Lu-Hf is a very beneficial isotope system to help date various geological events. With the use of ^{177}Hf, the ε_{Hf} values can be calculated, and help determine the age and source of the zircon.

Zircon's resistance to chemical weathering results in deposition into the ocean only occuring from very large scale erosional events. Sediment that is typically deposited out onto the ocean floor from smaller weathering events do not contain zircons. They tend to fall out onto the continental shelf due to their high specific gravity. When large scale erosion occurs, such as glacial activity, the zircons may be deposited further out into the ocean.

Antarctica is naturally broken up into eastern and western bedrock age jurisidctions by the Trans Antarctic Mountains. Western Antarctica is composed of younger bedrock in comparison to Eastern Antarctica. Eastern Antarctica is composed of ancient bedrock that has extremely nonradiogenic Nd values (Roy et al., 2007)(Figure 3). These unradiogenic values are a product of unstable ^{147}Sm decay over time to stable ^{143}Nd, and the ^{143}Nd/^{144}Nd ratio relative to bulk Earth (Scher et al., 2011). During a large weathering event on Antarctica, the bedrock would become eroded. Following the drainage basin paths, the sediment would flow into Prydz Bay, and out into the Southern Ocean vacinity.

The study site for this project is ODP Site 748 (58°26.45'S, 78°58.89'E, 1290m) on the central Kerguelen Plateau. This site was chosen because of its location on the eastern side of Antarctica and its vicinity to Prydz Bay. The

drainage divides indicate that a large portion of the eroded material from east Antarctica will flow through Prydz Bay. The weathered material could then be transported into the Kerguelen Plateau vicinity due to the Kerguelen Deep Western Bounday Current (Scher et al., 2011). The Kerguelen Plateau is a large igneous provence consisting of large amounts of mantle-derived magma that erupted from hotspot activity in the Indian Ocean (Frey et al., 2000).

CHAPTER 2: METHODS AND MATERIALS

The terrigenous fraction of the sediment samples were extracted following the methods established in Bayon et al. (2002). Approximately 5 grams of bulk sediment was weighed out into a polypropylene Nalgene bottle. The carbonate fraction was removed from the bulk sediment using a buffered acetic acid solution. The sediment was then rinsed 3x with 18 Ohm. The authigenic fraction was removed from the sediment using a 1M hydroxylamine hydroxide solution. The samples were then rinsed 3x and dried down. Following Krogh (1973) methods for Hafnium extraction, approximately 40mg of the samples are weighed out into Teflon vials and put into Teflon bombs with 4 mls of a HF and HNO_3 solution (3:1). The Teflon bomb was then placed into the metal bombing jacket and placed in an oven at $150^{O}C$ for 4 days. The samples were then removed from the bombs and dried.

After the bombing of the samples, the methods follow Hf dissolution and separation based on Munker et al. (2001) methods. The samples were brought up in 4ml of 6N HCl and dried down. This step was completed a total of three times. Next, the samples were brought up in 1ml of 3N HCl and dried down. The samples were then prepared and loaded onto the columns following Munker et al. (2001) methods.

For detrital Nd procedure, the methods followed Scher et al. (2009). After leaching, the 5 mg of sediment was weighed out into a Teflon vial. 4 ml of HNO_3

plus the weight of the sediment multiplied by 7.5 µl of HF was added to the sample. The Teflon vial was then placed on a hot plate at 170 ^{O}C for three days until the sediment is fully dissolved. The sample was then dried. 2ml of 6M HCl was added, and immediately dried down. The sample was then run on columns following the Scher et al. (2009) method. The samples were analyzed on a Thermo Neptune MC-ICP-MS in the Center for Elemental Mass Spectrometry Lab at The University of South Carolina.

CHAPTER 3: RESULTS

Table 1 contains the detrital Nd and Hf isotope data from ODP site 748B at the southern end of the Kerguelen Plateau. In order to compare the isotopes, the $\varepsilon_{Nd}(t)$, $\varepsilon_{Hf}(t)$, and $\delta^{18}O$ (Bohaty et al., 2003) data is plotted against age(Ma) (Figure 3.4).

748B $\varepsilon_{Nd}(t)$ and $\delta^{18}O$

There is a prominent $\varepsilon_{Nd}(t)$ shift during the late Eocene (Figure 3.4, top). Average $\varepsilon_{Nd}(t)$ values shift from -9.86 to a minimum value of -12.69 at 37.06 Ma and then back to around -9. At the same time, the benthic foraminifera *Cibicidoides praemundulus* $\delta^{18}O$ values (Figure 3.4, bottom) increase from a mean value of 1.25 ‰ to a peak $\delta^{18}O$ value of 1.71 ‰ at 37.06 Ma. The ε_{Nd} record shows a second, smaller, excursion beginning 36.67 Ma. ε_{Nd} values were -8 pre and post-excursion, with a minimum value of -11 during the excursion. The $\delta^{18}O$ foraminifera record shows a 0.3 ‰ increase before the ε_{Nd} decrease, beginning 36.81 Ma.

748B $\varepsilon_{Hf}(t)$

The results from $\varepsilon_{Hf}(t)$ show a small excursion to more unradiogenic $\varepsilon_{Hf}(t)$ values at the Bartonian/Priabonian boundary (Figure 3.4, middle). There is a second excursion at the same time as the second, smaller, $\varepsilon_{Nd}(t)$ shift.

748B Nd-Hf Arrays

In order to look for a zircon influence, the detrital $\varepsilon_{Nd}(t)$ and $\varepsilon_{Hf}(t)$ values were plotted along the terrestrial and seawater arrays (Figure 3.5). When the values were plotted along the arrays, the terrigenous samples plotted close to the seawater array. The average ε_{Hf} value is 2.10. There is a single point decrease at 39.98 Ma down to -2.83.

Table 3.1 Nd and Hf Isotope Data
119-748B-

core, section	interval (cm)	Depth (mbsf)	Age (Ma)	143Nd/144Nd	143/144 t	2SEM	eNd (0)	eNd(t)	2SEM	eHf (0)	εHf(t)	2SEM
15H-5	52-54	130.12	36.20	0.512203	0.512174	0.000003	-8.48	-8.16	0.07	2.82	3.50	0.12
15H-5	94-96	130.54								2.86	3.54	0.16
15H-6	12-14	131.22	36.37	0.512231	0.512202	0.000011	-7.93	-7.60	0.21	2.77	3.46	0.21
15H-6	12-14	131.22	36.37							2.34	3.02	0.11
15H-6	52-54	131.62	36.44	0.512206	0.512176	0.000004	-8.43	-8.10	0.08	2.60	3.28	0.10
15H-6	94-96	132.04	36.50	0.512205	0.512176	0.000008	-8.44	-8.11	0.15	2.00	2.68	0.11
15H-6	94-96	132.04	36.50	0.512174	0.512144	0.000006	-9.05	-8.72	0.12			
15H-6	134-136	132.44	36.52	0.512142	0.512112	0.000011	-9.68	-9.35	0.21	0.32	1.00	0.14
15H-7	22-24	132.82	36.55	0.512150	0.512121	0.000011	-9.51	-9.18	0.21	0.85	1.53	0.18
15H-7	42-45	133.02	36.56	0.512075	0.512046	0.000009	-10.98	-10.65	0.19			
15H-CC	2-4	133.23	36.58	0.512127	0.512097	0.000006	-9.98	-9.64	0.12	0.88	1.57	0.17
15H-CC	2-4	133.23	36.58	0.512134	0.512104	0.000007	-9.83	-9.50	0.13			
16H-1	47-49	133.57	36.62	0.512183	0.512154	0.000004	-8.87	-8.54	0.08			
16H-1	88-90	133.98	36.67	0.512195	0.512165	0.000009	-8.64	-8.30	0.17	1.68	2.36	0.11
16H-1	129-131	134.39	36.71	0.512195	0.512165	0.000009	-8.64	-8.30	0.18	7.13	7.81	0.23
16H-1	129-131	134.39	36.71							1.75	2.43	0.10
16H-2	37-39	134.8	36.75	0.512163	0.512133	0.000015	-9.27	-8.94	0.29			
16H-2	75-77	135.18	36.79	0.512163	0.512133	0.000005	-9.26	-8.93	0.11	4.30	4.99	0.18
16H-2	75-77	135.18	36.79	0.512152	0.512122	0.000008	-9.48	-9.15	0.17			
16H-2	118-120	135.61	36.84	0.512149	0.512119	0.000009	-9.55	-9.21	0.17			
16H-2	118-120	135.61	36.84	0.512156	0.512126	0.000006	-9.39	-9.06	0.11			
16H-3	13-15	136.06	36.89	0.512148	0.512118	0.000005	-9.55	-9.22	0.10			
16H-3	53-55	136.46	36.93	0.512134	0.512104	0.000006	-9.82	-9.49	0.11	0.87	1.57	0.13
16H-3	73-75	136.66	36.95	0.512120	0.512089	0.000003	-10.11	-9.80	0.06			
16H-3	93-95	136.86	36.98	0.512082	0.512052	0.000014	-10.85	-10.51	0.28	-3.53	-2.83	0.13
16H-3	93-95	136.86	36.98	0.512099	0.512069	0.000011	-10.52	-10.18	0.21			
16H-3	112-114	137.05	37.00	0.512085	0.512055	0.000007	-10.78	-10.45	0.14			
16H-3	112-114	137.05	37.00	0.512096	0.512065	0.000003	-10.58	-10.26	0.06			
16H-3	132-134	137.25	37.02	0.512067	0.512037	0.000009	-11.13	-10.80	0.17	-0.08	0.62	0.15
16H-4	5-7	137.48	37.04	0.512055	0.512025	0.000005	-11.37	-11.04	0.09			
16H-4	25-28	137.68	37.06	0.512006	0.511976	0.000008	-12.33	-11.99	0.16	1.41	2.11	0.47
16H-4	25-27	137.68	37.06	0.511970	0.511940	0.000011	-13.02	-12.69	0.21			
16H-4	25-27	137.68	37.06	0.511973	0.511942	0.000005	-12.98	-12.64	0.10			
16H-4	45-47	137.88	37.07	0.511981	0.511950	0.000007	-12.83	-12.49	0.13			
16H-4	65-67	138.08	37.07							-0.28	0.41	0.14

Table 3.2 Nd and Hf Isotope Data cont.
119-748B-

core, section	interval (cm)	Depth (mbsf)	Age (Ma)	143Nd/144Nd	143/144 t	2SEM	eNd (0)	eNd(t)	2SEM	eHf (0)	εHf(t)	2SEM
16H-4	65-67	138.08	37.07							2.21	2.91	0.31
16H-4	85-87	138.28	37.08	0.512057	0.512027	0.000012	-11.33	-10.99	0.23			
16H-4	105-107	138.48	37.09	0.512042	0.512012	0.000011	-11.62	-11.29	0.22	-0.27	0.42	0.17
16H-4	105-107	138.48	37.09	0.512035	0.512005	0.000012	-11.76	-11.42	0.23			
16H-4	125.5-127.5	138.685	37.11	0.512002	0.511972	0.000007	-12.41	-12.08	0.13	-1.05	-0.36	0.16
16H-4	145-147	138.88	37.13	0.512080	0.512050	0.000009	-10.88	-10.55	0.17	1.03	1.73	0.17
16H-5	14-16	139.07	37.15	0.512087	0.512057	0.000008	-10.74	-10.40	0.16	-0.05	0.65	0.16
16H-5	34-36.5	139.27	37.16	0.512108	0.512078	0.000009	-10.34	-10.01	0.18	1.39	2.09	0.14
16H-5	54-56	139.47	37.18	0.512115	0.512085	0.000007	-10.20	-9.86	0.14			
16H-5	72.5-76	139.655	37.20	0.512120	0.512089	0.000007	-10.11	-9.78	0.14			
16H-5	113-116	140.06	37.24	0.512097	0.512066	0.000010	-10.56	-10.22	0.19			
16H-5	134-136	140.27	37.26	0.512120	0.512089	0.000006	-10.11	-9.77	0.11			
16H-6	3-5	140.46	37.28	0.512178	0.512147	0.000004	-8.98	-8.64	0.07			
16H-6	23-25	140.66	37.30	0.512139	0.512109	0.000007	-9.73	-9.39	0.14			
16H-6	42-45	140.85	37.32	0.512125	0.512095	0.000008	-10.00	-9.67	0.15			
16H-7	13-15	141.28	37.36	0.512087	0.512057	0.000011	-10.74	-10.40	0.22			
16H-7	53-55	141.68	37.40	0.512065	0.512034	0.000012	-11.18	-10.84	0.24			
16H-7	53-55	141.68	37.40	0.512068	0.512038	0.000006	-11.11	-10.78	0.11			
17H-1	6-8	142.66	37.48	0.512081	0.512050	0.000017	-10.87	-10.53	0.33			
17H-1	48-50	143.08	37.52	0.512115	0.512085	0.000018	-10.20	-9.86	0.35			

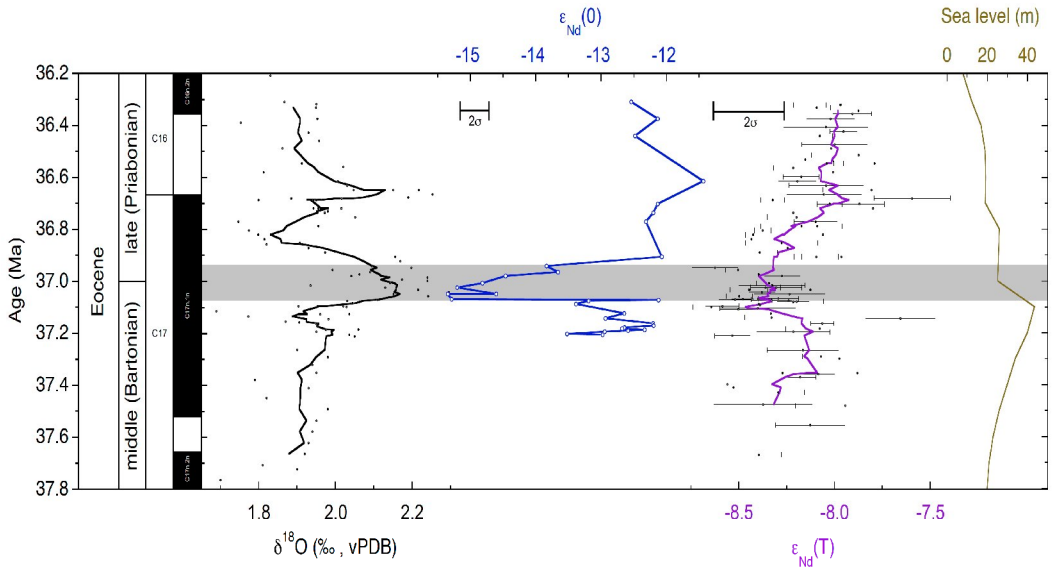

Figure 3.1 Bartonian/Priabonian boundary (gray bar) cool event with supporting evidence from foraminifera $\delta^{18}O$ increase (Bohaty, personal communication), detrital ε_{Nd} decrease, fish tooth ε_{Nd} decrease (Scher et al., in prep), and eustatic sea level decrease (Miller et al., 2005).

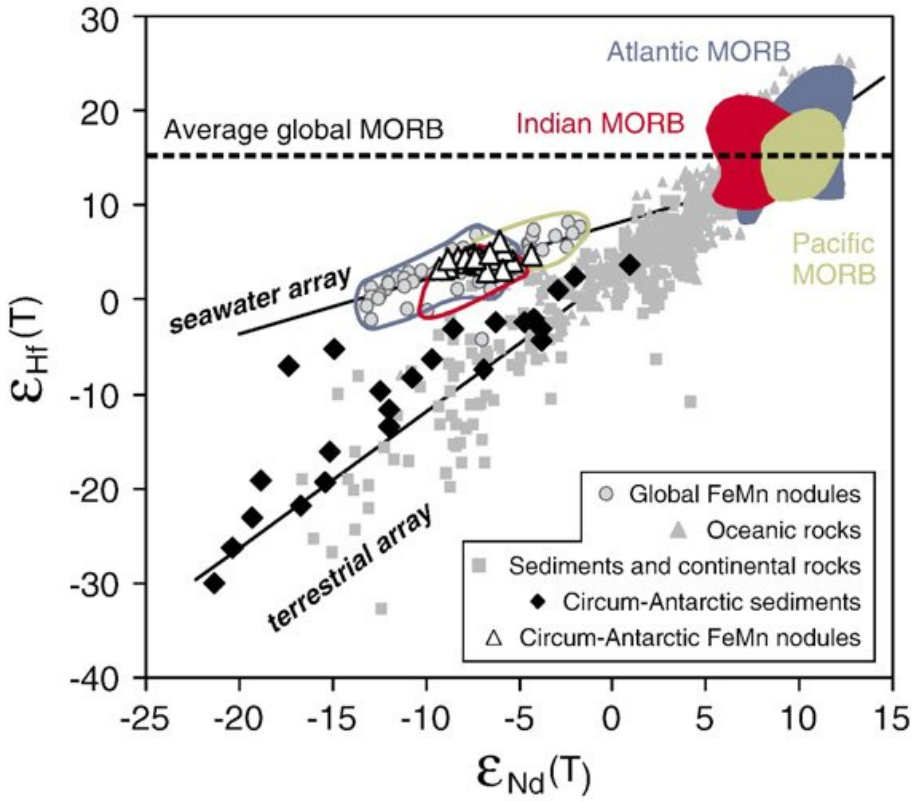

Figure 3.2 Plot of global Nd-Hf isotopes with components included in the Seawater and Terrestrial Array (van de Flierdt et al., 2007).

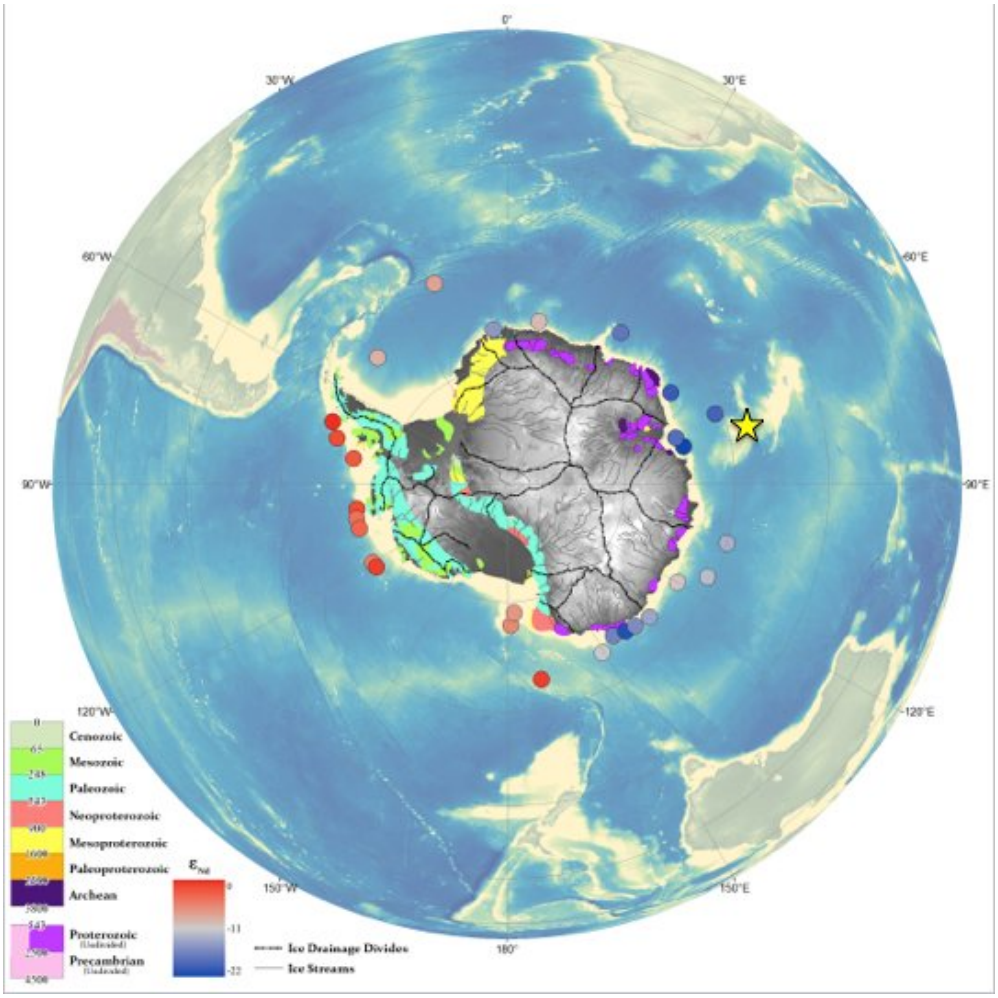

Figure 3.3 Map of Antarctica with ODP Site 748 indicated by yellow star. Circles surrounding Antarctica indicate core-top ε_{Nd} values (Roy et al., 2007 and van de Flierdt et al., 2007). Basement rock color signifies age (Kirkham and Chorlton, 1995 and Roy et al., 2007).

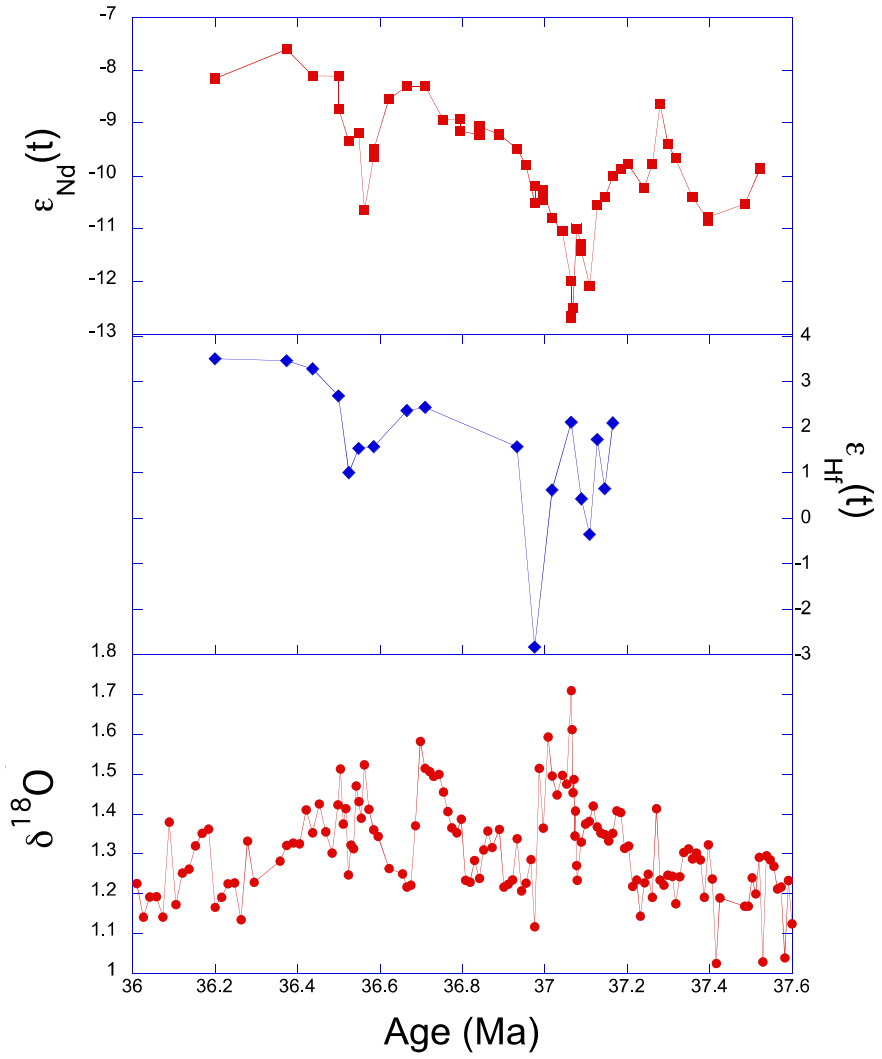

Figure 3.4 Detrital $\varepsilon_{Nd}(t)$ (top), detrital $\varepsilon_{Hf}(t)$ (middle), and $\delta^{18}O$ (bottom) (Bohaty et al., 2003) from ODP 748B

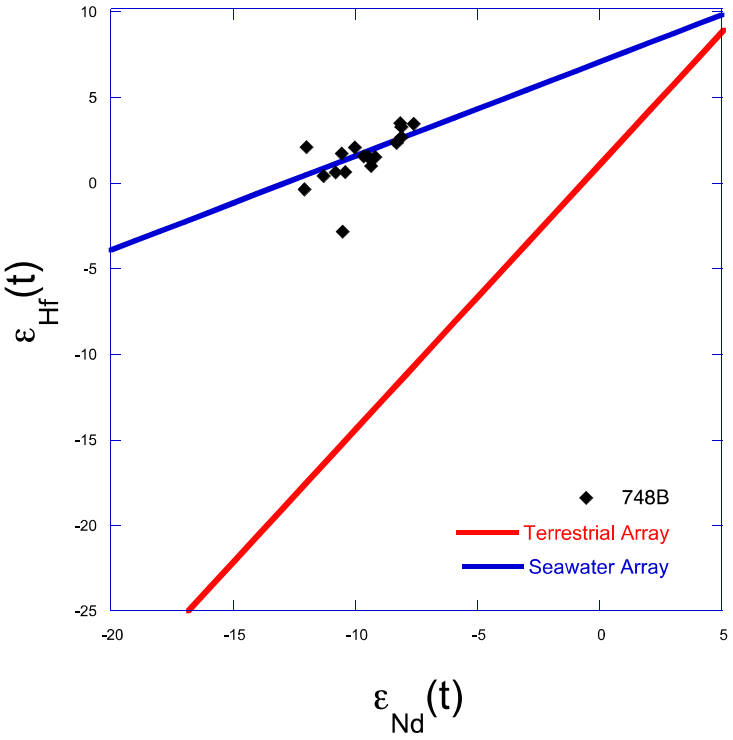

Figure 3.5 Detrital ε_{Nd} and ε_{Hf} values from ODP 748B cross-plotted along with the terrestrial array (blue)(Vervoort, 1999; van de Flierdt et al., 2006) and seawater array (red)(Albarede et al., 1998; van de Flierdt et al., 2007; Stichel et al., 2011)

Chapter 4: DISCUSSION

Terrigenous sediment is delivered to the deep sea by three primary mechanisms, outlined in the classic work of Emiliani and Milliman (1966); 1) settling from the water column, 2) bottom transport by gravity flows, or 3) transportation by geostrophic bottom currents. Below these mechanisms will be evaluated in the context of terrigenous supply to central Kerguelen Plateau.

Material settling through the water column could come from aeolian or extraterrestrial sources. Both of these sources are unlikely to account for the observed radiogenic isotope variability on Kerguelen Plateau. First, both of these sources would likely produce more radiogenic (i.e., positive ε_{Nd} values). Dust sources to the Indian sector of the Southern Ocean are predominantly carried by the westerly winds, derived from juvenile sources in Patagonia and the Antarctic Peninsula. The signature of this material is seen west of 40˚ W (Hegner et al., 2007) and rapidly diminishes to the east toward the study site.

The most likely scenario of terrigenous sediment deposition onto the central Kerguelen Plateau is from the transportation of suspended material from turbidity currents by geostrophic bottom currents. Deep Western Boundary Currents are bathymetrically constrained and are considered permanent features of the ocean, albeit modified by plate configurations. Weathered material from Antarctica flows into the Southern Ocean via ice flows/rivers. In the Eocene weathered and eroded material was likely transported to the continental shelf by

rivers draining the Lambert Graben, which discharges in Prydz Bay. The Kerguelen Plateau is in the vicinity of Prydz Bay, a major outlet of weathered material from Antarctica. Antarctic bedrock transported by pre-glacial rivers is deposited onto the continental shelf and upper slope. Sediment accumulating at the shelf/slope break becomes unstable and collapses, resulting in a cascade of sediment down the slope under the influence of gravity, and into the deep sea. Once terrestrial material from these gravity flows were suspended, the Kerguelen Deep Western Boundary Current could conceivably transport silt in suspension to the study area (Fukamachi et al., 2010). This transport would bring the older, unradiogenic, bedrock eroded from Antarctica onto the Kerguelen plateau, resulting in the excursion to more unradiongenic values (Figure 3.4). The volcanic material from the Kerguelen Islands, to the north of the study site, may have also contributed to the terrigenous fraction. Thus, Kerguelen Plateau has less radiogenic sediment sources to the south and more radiogenic sediment sources to the north. Thus, the radiogenic isotopic composition of terrigenous sediment on Kerguelen Plateau is likely to be somewhat dependent on latitude.

Previous results from ODP Site 738B during the Bartonian/Priabonian boundary indicate an increase in weathering/erosion from Antarctica. The results from this study suggest similar conclusions. Figure 3.4 shows a ε_{Nd} excursion from -9.86 down to -12.69 at 37.06 Ma, a time when the Earth is presumed to be ice-free. This excursion depicts a change in sediment source that caused an influx of nonradiogenic material to be deposited onto central Kerguelen Plateau. It is likely that glacial grinding on Antarctica's ancient eastern bedrock is

influenced the source of the material flux during the late Eocene. During the same period as the ε_{Nd} excursion, there is an increase in benthic foraminifera $\delta^{18}O$ values from 1.25 ‰ to 1.71 ‰ (Bohaty et al., 2003)(Figure 3.4). The combination of the ε_{Nd} value drop along with the $\delta^{18}O$ increase provides evidence of a change in source material being deposited into the Southern Ocean during a time of global cooling or ice sheet growth.

Coupled Nd-Hf of central Kerguelen Plateau sediments revealed two findings; 1) detrital sediment from Eocene sections plot parallel to the seawater array, and 2) a single data point during the recovery (36.98 Ma) is shifted towards the terrestrial array (Figure 3.5). Two possible explanations for the results are from, 1) a change in the weathering regime, or 2) dilution of the less radiogenic signal during transport.

A change in the weathering mechanism could be signified by the Nd-Hf data plotting along the seawater array. There is indication of weathering change from predominantly chemical to mechanical near the Bartonian/Priabonian boundary. A change to a less mechanical weathering style would be reflected by the coupled data plotting along the seawater array. During the recovery to pre-excursion values, there is a single point shift towards the terrestrial array. This data point could signify an increase in mechanical weathering, depositing zircons into the Southern Ocean. As discussed previously, coupled Nd-Hf data for present-day circum-Antarctic sediments plot along the terrestrial array, suggesting that congruous weathering of minerals hosting Hf is accommodated by intense mechanical weathering by Antarctic ice sheets. It is thus remarkable

that Eocene sediments plot along the seawater array as it suggests that the radiogenic isotopic composition of sediments shed from Antarctica is dependent on the style of weathering.

A second scenario for the lack of terrestrial array shift is that the eroded material from Antarctica was modified by grain size/density sorting during transport within the DWBC out to the central Kerguelen Plateau. Coupled Nd-Hf data from Site 1166 (van de Flierdt, personal communication) showed detrital sediment from the Eocene that plotted along the terrestrial array. Site 1166 is located in the mouth of Prydz Bay and would record ε_{Hf} values that are highly influenced by zircons, before possible dilution.

There is another time period where a second, smaller, excursion is recorded in the detrital sediment from ODP 748B. At approximately 36.5 Ma, there is a decrease in $\varepsilon_{Nd}(t)$ values from -9.5 down to -11. At the same time, there is a decrease in $\varepsilon_{Hf}(t)$. Slightly before the ε_{Nd} and ε_{Hf} excursions, there is an increase in the foraminifera $\delta^{18}O$ beginning 36.8 Ma. These excursions are smaller than the event at the Bartonian/Priabonian boundary but they are well recorded in the terrigenous samples.

CHAPTER 5: CONCLUSION

A detailed history of weathering on Eastern Antarctica at the Bartonian/Priabonian boundary has been compiled from detrital ε_{Nd}, ε_{Hf}, and foraminifera $\delta^{18}O$ values. The results show two pulses, with the larger pulse approximately 37 Ma and a younger, smaller, excursion approximately 35.5 Ma. These two pulses are signified by a change in weathering material coinciding with an increase in global cooling/ice sheet growth. Detrital ε_{Hf} values reveal a small change in weathering style, to more mechanical, at these two excursions. When the ε_{Hf} and ε_{Nd} data was cross-plotted, the values plotted in congruence with the seawater array, providing insight on the composition of the eroded material into the Kerguelen Plateau area. These factors extracted from ODP Site 748B provide supporting evidence of the onset of high elevation ice sheets on Antarctica 37 Ma.

REFERENCES

Albarède, F., Simonetti, A.,Vervoort, J.D.,Blichert-Toft, J., Abouchami,W.,(1998) A Hf–Nd isotopic correlation in ferromanganese nodules. Geophys. Res. Lett. 25, 3895–3898.

Bayon, Gunter, C. R. German, R. M. Boella, J. A. Milton, R. N. Taylor, and R. W. Nesbit (2002) An Improved Method for Extracting Marine Sediment Fractions and Its Application to Sr and Nd Isotopic Analysis. Chemical Geology 187, 179-99.

Bohaty, Steven M; Zachos, James C (2003) Carbon and oxygen isotopic compositions of Cibicidoides spp. and fine fraction separates (<10 μm) from ODP Holes 113-689B, 119-738B, and 120-748B.

Coxall, Helen K. (2005) Rapid stepwise onset of Antarctic glaciation and deeper calcite compensation in the Pacific Ocean. Nature 433.702, 53-57.

Edgar, Kirsty M., Paul A. Wilson, Philip F. Sexton, and Yusuke Suganuma. (2007) No Extreme Bipolar Glaciation during the Main Eocene Calcite Compensation Shift. Nature 448.7156. 908-11.

Emiliani C, Milliman JD (1966) Deep-sea sediments and their geological record. Earth Science Reviews 1:105–132

Faure, Gunter. Principles of Isotope Geology. 2nd ed. New York: Wiley, 1986.

Frey, F.A., M.F. Coffin, P.J. Wallace, D. Weis, X. Zhao, S.W. Wise Jr., V. Wähnert, D.A.H. Teagle, P.J. Saccocia, and D.N. Reusch. (2000) Origin and Evolution of a Submarine Large Igneous Province: The Kerguelen Plateau and Broken Ridge, Southern Indian Ocean." Earth and Planetary Science Letters 176.1. 73-89.

Fukamachi, Y., S. R. Rintoul, J. A. Church, S. Aoki, S. Sokolov, M. A. Rosenberg, and M. Wakatsuchi. (2010) Strong Export of Antarctic Bottom Water East of the Kerguelen Plateau. Nature Geoscience 3.5. 327-31.

Hegner, E., H. J. Dauelsberg, M. M. Rutgers Van Der Loeff, C. Jeandel, and H. J. W. De Baar. (2007) Nd Isotopic Constraints on the Origin of Suspended Particles in the Atlantic Sector of the Southern Ocean." Geochemistry Geophysics Geosystems 8.10.

Hickey, R.L., Frey, F.A., Gerlach, D.C., (1986) Multiple sources for basaltic arc rocks from the southern volcanic zone of the Andes (34°–41°S): Trace element and isotopic evidence for contributions from subducted oceanic crust, mantle, and oceanic crust J. Geophys. Res., 91 pp. 5963–5983

Kinny, P. D. (2003) Lu-Hf and Sm-Nd Isotope Systems in Zircon. Reviews in Mineralogy and Geochemistry 53.1. 327-41.

Krogh, T. (1973) A Low-contamination Method for Hydrothermal Decomposition of Zircon and Extraction of U and Pb for Isotopic Age Determinations. Geochimica Et Cosmochimica Acta 37.3. 485-94.

Lyle, Mitchell, Annette Olivarez Lyle, David Rea, and Jan Backman. (2005) The Stuttering Greenhouse and Cenozoic Carbonate Compensation Depth. Goldschmidt Conference Abstracts 69.10.

Martin, E.E., Blair, S.W., Kamenov, G.D., Scher, H.D., Bourbon, E., Basak, C., and Newkirk, D.N. (2010) Extraction of Nd isotopes from bulk deep sea sediments for paleoceanographic studies on Cenozoic time scales. Chemical Geology 266(3-4), 414-431.

Miller, K.G., R.G. Fairbanks and G.S. Mountain, (1987) Tertiary oxygen isotope synthesis, sea level history, and continental margin erosion : Paleoceanography, 2(1):1–19, Deep Sea Research Part B. Oceanographic Literature Review, 34.9. 760-761,

Miller, K. G. (2005) The Phanerozoic Record of Global Sea-Level Change. Science 310.5752 1293-298.

Münker, Carsten, Stefan Weyer, Erik Scherer, and Klaus Mezger (2001) "Separation of High Field Strength Elements (Nb, Ta, Zr, Hf) and Lu from Rock Samples for MC-ICPMS Measurements." Geochemistry Geophysics Geosystems 1.12.

Munn, Gabrielle. (2011) Chemical Weathering History of Antarctica during a Late Eocene Glacial Event. Diss. University of South Carolina.

Pagani, M. (2005) Marked decline in atmospheric carbon dioxide concentrations during the Paleogene. Science 309.5734. 600-603.

Roy, M., T. Vandeflierdt, S. Hemming, and S. Goldstein. (2007) 40Ar/39Ar Ages of Hornblende Grains and Bulk Sm/Nd Isotopes of Circum-Antarctic Glacio-marine Sediments: Implications for Sediment Provenance in the Southern Ocean. Chemical Geology 244.3-4. 507-19.

Scher H.D. and Delaney M.L. (2009) Breaking the glass ceiling for high

resolution Nd isotope records in paleoceanography. Chemical Geology.

Scher, Howie D., and Margaret L. Delaney. (2010) Breaking the Glass Ceiling for High Resolution Nd Isotope Records in Early Cenozoic Paleoceanography. Chemical Geology 269.3-4 (2010): 329-38.

Scher, H. D., Bohaty, S. M., Zachos, J. C., & Delaney M. L. (2011). Two-stepping into the icehouse: East Antarctic weathering duringprogressive ice-sheet expansion at the Eocene–Oligocene transition. Geology, 39 (4), 383-386.

Stichel, T., Frank, M., Rickli, J., Haley, B. A., (2012) The hafnium and neodymium isotope composition of seawater in the Atlantic sector of the Southern Ocean. Earth and Planetary Science Letters 317-318, 282-294.

Van de Flierdt, T., S. Goldstein, S. Hemming, M. Roy, M. Frank, and A. Halliday. (2007) Global Neodymium–hafnium Isotope Systematics — Revisited. Earth and Planetary Science Letters 259.3-4 432-41.

Vervoort, J.D., Patchett, P.J., Blichert-Toft, J., Albarède, F., (1999) Relationships between Lu–Hf and Sm–Nd isotopic systems in the global sedimentary systems. Earth Planet. Sci. Lett. 168, 79–99.

White, W., J. Patchett, and D. Benothman. (1986) Hf Isotope Ratios of Marine Sediments and Mn Nodules: Evidence for a Mantle Source of Hf in Seawater. Earth and Planetary Science Letters 79.1-2. 46-54.

Zachos, James C., William A. Berggren, Marie-Pierre Aubry, and Andreas Mackensen. (1992) Isotope and Trace Element Geochemistry of Eocene and Oligocene Foraminifers from Site 748, Kerguelen Plateau. Proceedings of the Ocean Drilling Program, Scientific Results 120.

Zachos J, Pagani M, Sloan L, Thomas E, Billups K. (2001) Trends, rhythms, and aberrations in global climate 65 Ma to present. Science, 292:686-693.